J Mater Sci (2012) 47:121–131
DOI 10.1007/s10853-011-5773-4

Relationship between rheological and surface properties for the sintering process of polymers

Jean-Damien Muller · Khalid Lamnawar · Abderrahim Maazouz

Received: 24 May 2011 / Accepted: 6 July 2011 / Published online: 23 July 2011

Abstract The aim of the present work is to examine the effect of the rheological behaviour and surface properties on the sintering of various polymers. Model polymers, liquid at room temperature and commercials materials with different viscosities and structures are used. Zero-shear viscosities and relaxation times are extracted from rheological curves. The surface tension of the materials is measured by the sessile drop method when possible. The sintering of two particles put in close vicinity is recorded using a CCD camera at regular intervals time. Two substrates with different surface tension are employed. The effects of viscosity, surface tension and relaxation time on the sintering kinetics are discussed.

Introduction

Rapid manufacturing and rotational moulding process are the most adapted method to produce large hollow and complex plastic parts without weld lines. They involve four steps: (1) melting of the polymer powder in the mould, (2) coalescence of the particles, (3) densification of the melt bed and (4) cooling period. It appears that one of the main physical phenomena that govern the cycle time and the quality of dissolution of bubble gas into the polymer melt is the coalescence [1], what we can also call sintering.

The sintering phenomenon has been first studied for metals and ceramic materials [2, 3] and then the approach has been extended to polymers [4]. Various models have been proposed in this area. Frenkel [5] described the rate of coalescence occurring by viscous flow promoted by surface tension for two Newtonian spherical particles having the same diameter, during the early stages of sintering. However, such a model violates the continuity equation, which was corrected later by Eshelby [6]. Extension of Frenkel's model was given by Hopper [7].

Pokluda et al. [8] extended the Eshelby–Frenkel approach to include the complete coalescence process of two spherical particles as illustrated in Fig. 1. Recently, Bellehumeur et al. [9] improved Pokluda model so as to better fit the experimental results of the polypropylene–ethylene copolymer sintering. The Bellehumeur sintering model has used the upper convected Maxwell model [10], assuming quasi-steady state flow, to obtain a non-linear differential equation. In this model, the sintering rate is a function of the material relaxation time and the characteristic sintering time: $\eta_0 r_0/\gamma$, where η_0 is the zero-shear viscosity, r_0 the initial particle radius and γ the surface tension. The model can be written as follow:

$$8(\beta\lambda K_1\theta')^2+\left(2\beta\lambda K_1+\frac{\eta_0 r_0}{\gamma}\frac{K_1^2}{K_2}\right)\theta'-1=0 \quad (1)$$

K_1 and K_2 are geometrical parameters given by:

$$K_1=\frac{\sin\theta}{(1+\cos\theta)(2-\cos\theta)} \quad (2)$$

$$K_2=\frac{2^{-5/3}\cos\theta\sin\theta}{(1+\cos\theta)^{4/3}(2-\cos\theta)^{5/3}} \quad (3)$$

J.-D. Muller · K. Lamnawar · A. Maazouz
Université de Lyon, 69361 Lyon, France

J.-D. Muller · K. Lamnawar · A. Maazouz (✉)
CNRS, UMR 5223, Ingénierie des Matériaux Polymères, INSA Lyon, 69621 Villeurbanne, France
e-mail: abderrahim.maazouz@insa-lyon.fr

A. Maazouz
Hassan II Academy of Science and Technology, Rabat, Morocco

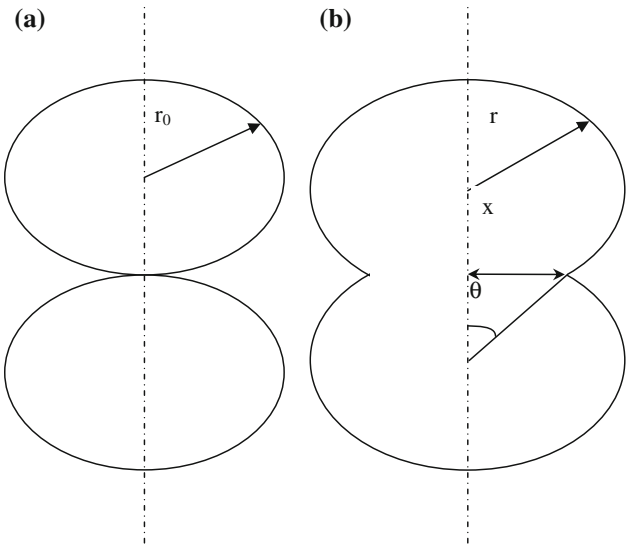

Fig. 1 Geometrical illustration of the sintering process of two drops at **a** $t = 0$ s and **b** $t > 0$ s. The parameters r, x and θ represent the radius, the neck radius and the sintering angle, respectively

θ is designed as the sintering angle as illustrated in Fig. 1. β is the Maxwell coefficient that takes the value $+1$ for the upper convected Maxwell model (UCM). More recently, an effort was made to develop a model which takes into account the transient rheology [11].

The aim of this work is first to study the sintering process from a fundamental point of view thanks to model fluids, then to use commercial materials used for rotational moulding. Various substrates were employed to explore the effect of the interfacial tension. The influence of rheological properties of materials was also examined.

Experimental

Materials

Nine model fluids were employed to better understand the sintering process: 3 poly(dimethylsiloxanes) PDMS, 2 polybutenes PB and 4 Boger fluids [12]. These fluids are a mix of a highly viscous polymer and a highly elastic one. We used here a PB as viscous polymer, and a polyisobutylene as the elastic component. The amount of PIB and the type of PB controls the elasticity of the BF's or their viscosity. Tables 1 and 2 give the nomenclature of the 9 fluids. All are liquid at room temperature.

5 industrial polymers were also studied: a copo(ethylene–propene) designed as Co-PEPP, two polypropylenes PP and PP-G, and two polyethylenes PE and PE-G. PP-G and PE-G are grafted with a chemical function which makes them compatible with polyamide, in order to produce multilayer parts for example.

Table 1 Zero-shear viscosity at 25° of the 3 PDMS and the 2 PBs

Sample	Zero-shear viscosity (Pa s) at 25 °C
PDMS1	10.6
PDMS2	28.9
PDMS3	80.8
PB1	23
PB2	502

Table 2 Composition of the various prepared Boger fluids

Sample	% Kerosene (solvent)	% Polyisobutylene (polymer)	% Polybutene (polymer solvent)
BF1	6.98	0.22	92.8 (PB1)
BF2	6.2	0.8	93 (PB1)
BF3	6.98	0.22	92.8 (PB2)
BF4	6.2	0.8	93 (PB2)

Surface tension measurements

Surface tensions were measured by sessile drop method. For model fluids, a drop of the material was deposited successively on three substrates of surface tension known. Contact angles at 25 °C between the fluid and its substrate were measured using images analyses software. We easily deduce the polar and non-polar parts of each fluid.

The surface tension measurement for Co-PEPP requires only one non-polar substrate. This kind of material is well-known to have a polar part equal to zero. The measurements were conducted ranging from 180 to 220 °C on a PTFE substrate. A polymer particle was deposited on it. The equilibrium of the molten polymer was observed before acquiring of the contact angle.

The equipment available at the laboratory cannot measure surface tension of highly viscous or elastic polymers. Values for PE, PE-G, PP and PP-G were also estimated by surface tension found in the literature. All of them have been reduced to a temperature of 200 °C.

Rheological tests

Rheological behaviours of model fluids have been observed. Tests were performed with a stress-controlled rotational rheometer AR100 from TA Instruments, with a cone and plate geometry. To obtain the largest range of frequencies, the tests were carried out from 25 to 65 °C. A master curve is plotted for a reference temperature of 25 °C using time–temperature superposition procedure. Newtonian viscosities and relaxation times at 25 °C for each fluid are deduced from this curve.

Rheological measurements for industrial polymers were performed using a strain-controlled rotational rheometer ARES from TA Instruments with a plate and plate geometry. Rheological properties of Co-PEPP were explored on a range of temperature from 180 to 230 °C. Rheological behaviour for the other materials was only tested at 200 °C, which is the sintering tests temperature chosen. Newtonian viscosities and relaxations times were calculated for each temperature.

Sintering experiments

The sintering experiments were conducted on a regulated hot stage on which the drops or the particles were deposited. A Zeiss binocular and a Pantera CCD camera linked to a computer allow to record images at regular intervals.

The sintering experiments were carried out at 25 °C for model fluids. Because of their relatively low viscosities, the drops adopt more or less instantaneously a spherical shape. This eases the sintering kinetics measurements at short times. 2 substrates with different surface tensions were used to observe the effect of the interfacial tension.

The sintering tests were performed at 195 and 225 °C for Co-PEPP. This will allow us to examine both effect of viscosities and relaxation times for industrial materials. 2 substrates with different surface tensions were also used. Finally, the sintering of PE, PE-G, PP and PP-G was observed at 200 °C. The same substrates than those used for Co-PEPP polymer have been employed.

All tests were repeated at least three times to ensure reproducibility. The results presented are the mean of the three tests since it decreases the experimental error (4%).

Results and discussion

Surface tension

Surface tension was evaluated for the all used samples. The contact angles between the liquids and three substrates were measured to determine the polar, γ_L^p, and the dispersive, γ_L^d, components of the liquid surface tension. When considering a liquid drop of surface tension γ_L on a solid substrate of surface tension γ_S, the equilibrium at the triple point can be written as:

$$\gamma_S = \gamma_{SL} + \gamma_L \cos\alpha \tag{4}$$

γ_{SL} is the interfacial tension between the liquid and the substrate and α the contact angle. According to Owens and Wendt [13], γ_{SL} can be expressed as:

$$\gamma_{SL} = \gamma_S + \gamma_L - 2\left(\gamma_S^d\gamma_L^d\right)^{1/2} - 2\left(\gamma_S^p\gamma_L^p\right)^{1/2} \tag{5}$$

According to Eqs. 2 and 3, this leads to:

$$\gamma_L(1+\cos\alpha) = 2\left(\gamma_S^d\gamma_L^d\right)^{1/2} + 2\left(\gamma_S^p\gamma_L^p\right)^{1/2} \tag{6}$$

In the above equation, the values of γ_S^d, γ_S^p and are known for each used substrate. This equation can be rewritten as follow:

$$\frac{(1+\cos\alpha)}{2\sqrt{\gamma_S^d}} = \frac{1}{\gamma_L}\sqrt{\gamma_L^p}\sqrt{\frac{\gamma_S^p}{\gamma_S^d}} + \frac{1}{\gamma_L}\sqrt{\gamma_L^d} \tag{7}$$

By plotting:

$$\frac{(1+\cos\alpha_i)}{2\sqrt{\gamma_{S_i}^d}} = f\left(\sqrt{\frac{\gamma_{S_i}^p}{\gamma_{S_i}^d}}\right) \tag{8}$$

where i is the number of substrate, the polar and the dispersive components of the liquid can be easily determined from the above expressions. The obtained results are given with an average error of ±0.2 mN/m.

Table 3 represents the surface tension measured for model fluids. The substrates used are glass, aluminium and PTFE. As we can see in column 5, polar parts can be neglected. Measurements can be achieved on a single nonpolar substrate (PTFE). This improves the accuracy. Surface tension can be simply estimated by:

$$\gamma_L = \frac{4\gamma_S}{(1+\cos\alpha)^2} \tag{9}$$

Surface tension of the three PDMS is quite similar. The two PB's show different surface tension. The surface tension of PB1 is 26.3 mN/m whereas that of PB2 is 27.4 mN/m. BF1 and BF2 have a surface tension quite similar to that of their matrix (PB1) and value of BF3 and BF4 is quite identical to that of PB2.

The surface tension of Co-PEPP is calculated at each test temperature according to Eq. 9. A small flow of an inert gas was necessary to prevent thermal degradation of the material. Table 4 gives the results obtained. The surface tension varies from 22.8 mN/m at 180 °C to 19.6 mN/m at 220 °C. These values are in accordance with typical results for a polypropylene [14]. The surface tension decreases linearly with the increase of the temperature with $d\gamma/dT = -0.08$ mN/m/°C. Such values are found in the literature too.

As it was previously mentioned, the equipment in the laboratory does not allow us to measure surface tension of highly viscous or elastic materials. Kwak et al. [15] have measured the surface tension of a PE. The value at 200 °C is 21.5 mN/m. According Wu [16], the surface tension of a grafted PE, comparable with our PE-G, is 23.3 mN/m at 200 °C. The value given by Hata and Kasemura [17] for a PP at 200 °C is 19.3 mN/m. We did not found any data for a grafted PP. In first approximation, we can also consider that the surface tension of PP-G is 19.3 mN/m at 200 °C.

Table 3 Surface tension values for model fluids obtained with 3 substrates (columns 2 trough 4) as well as merely 1 non-polar substrate (column 6)

Sample	Measurements with 3 substrates: PTFE, aluminium and glass at 25 °C			Contribution of polar part γ_L^p/γ_L (%)	Measurements with only PTFE at 25 °C $\gamma_L^d = \gamma_L$ (mN/m)
	γ_L^p (mN/m)	γ_L^d (mN/m)	γ_L (mN/m)		
PDMS1	0.6	22.4	23.0	2.8	23.3
PDMS2	0.5	23.1	23.6	2.3	23.8
PDMS3	0.6	22.7	23.3	2.6	23.6
PB1	0.3	26.1	26.4	1.1	26.3
PB2	0.2	27.6	27.8	0.7	27.4
BF1	0.2	26.3	26.5	0.8	26.5
BF2	0.4	26.1	26.5	1.5	26.3
BF3	0.2	27.3	27.5	0.7	27.2
BF4	0.3	27.3	27.6	0.9	27.3

The contribution of the polar component to the surface tension is displayed in column 5

Table 4 Surface tension values at several temperatures for Co-PEPP

Temperature (°C)	183	190	194	199	207	213	218	222
Surface tension (mN/m)	22.8	22.4	21.9	21.4	20.9	20.3	20.2	19.6

The relaxation times were calculated with the Cole–Cole method

Rheological properties

Figures 2 and 3 report the complex shear viscosity as a function of frequency for PDMS and PB samples at 25 °C. All samples present a large Newtonian plateau followed by a small decrease in viscosity at high frequencies mainly for large molecular weight samples. However, up to 80 rad/s, all the samples behave as Newtonian liquids. Beyond this value PDMS3 and PB2 show a decrease in viscosity as a function of frequency (frequency-thinning behaviour). Newtonian viscosities and relaxation times measured are shown in Table 5.

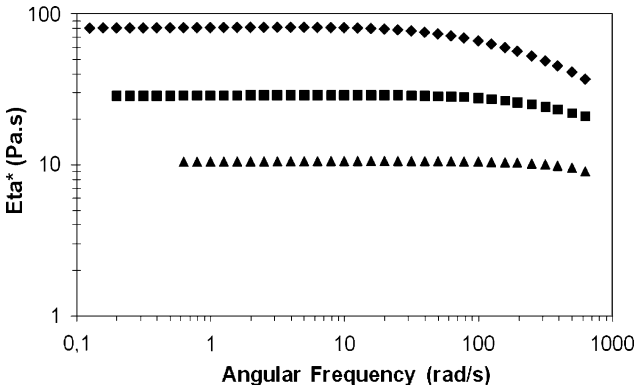

Fig. 2 The complex viscosity modulus vs the frequency for PDMS1 (*triangle*), PDMS2 (*square*) and PDMS3 (*diamond*) at 25 °C

Figures 4 and 5 show the variation of the storage shear modulus and the complex shear viscosity as a function of frequency for BF1, BF2 and BF3, BF4, respectively. The two sets of samples differ in the nature of PB used as a

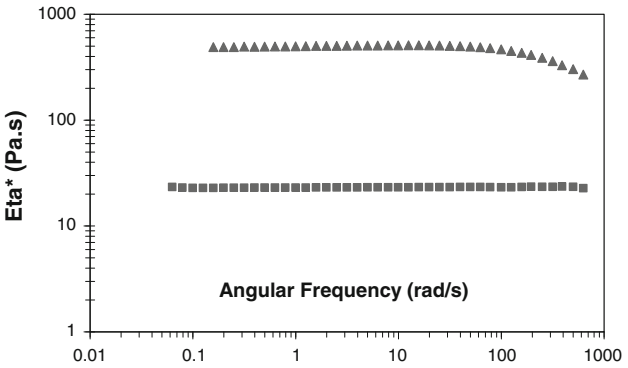

Fig. 3 Complex shear viscosity vs frequency for PB1 (*square*) and PB2 (*triangle*) at 25 °C

Table 5 Rheological characteristics for PDMS and PB samples at 25 °C

Fluid	Eta* (Pa s)	λ (s)
PDMS1	10.6	1.5×10^{-4}
PDMS2	28.9	1.5×10^{-3}
PDMS3	80.8	3.1×10^{-3}
PB1	23	10^{-5}
PB2	502	2.6×10^{-3}

matrix (refer to Table 2). BF1 and BF2 samples exhibit quite the same behaviour as a function of frequency with a clear Newtonian plateau in the low-frequency region (viscosity is constant and G' is almost zero) with a zero-shear viscosity of about 17 Pa s for BF1 and of about 30 Pa s for BF2, followed by a sharp decrease in viscosity before reaching a second plateau at high frequencies. Such a decrease starts at approximately 0.2 rad/s and extends to 50 rad/s.

The second series (BF3 and BF4) shows a completely different trend with a Newtonian viscosity in the low-frequency region followed by a smooth transition towards a second plateau for intermediate frequencies. At approximately 70 rad/s, the viscosity shows a second transition with a decrease in viscosity with frequency. The difference in behaviour of the two series is due to the difference in the behaviour of their polymer matrix. In fact, in comparison with Fig. 3, the high frequency-thinning behaviour (similar to shear-thinning) observed in BF3 and BF4 can be linked with that of PB2. In contrast, PB1 did not show any frequency-thinning above 20 rad/s (Fig. 4) and therefore the corresponding Boger fluids, BF1 and BF2 show a second plateau at high frequencies.

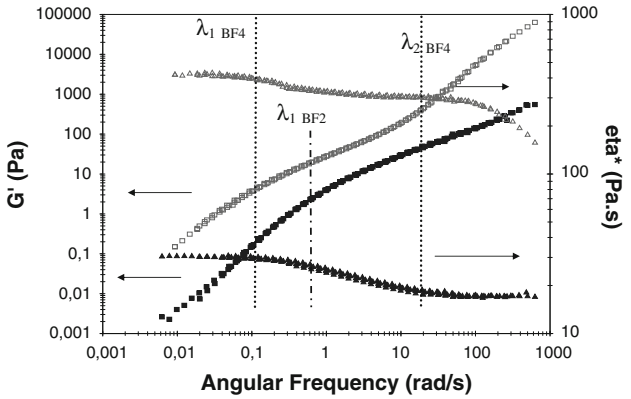

Fig. 4 The rheological behaviour of BF2 (*filled triangle*, *filled square*) and BF4 (*open triangle*, *open square*). The elastic modulus (*filled square*, *open square*) is reported on the left axis, whereas the complex viscosity is displayed on the right axis (*filled triangle*, *open triangle*)

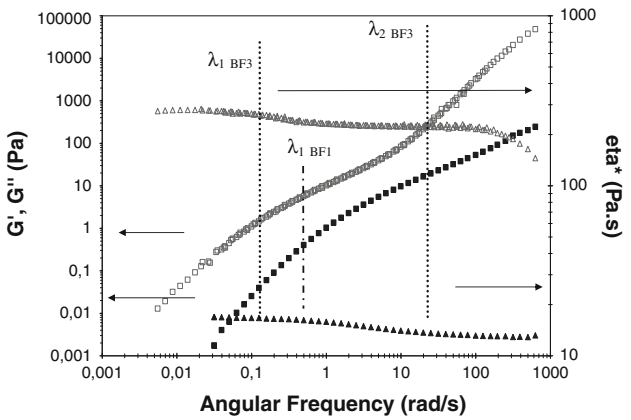

Fig. 5 The rheological behaviour of BF1 (*filled triangle*, *filled square*) and BF3 (*open triangle*, *open square*). The elastic modulus (*filled square*, *open square*) is reported on the left axis, whereas the complex viscosity is displayed on the right axis (*filled triangle*, *open triangle*)

Characteristic relaxation times were determined from the Cole–Cole diagram. The results are shown in Table 6. We observe that the relaxation time $\lambda 1$ is strongly dependent on PIB concentration, as it increases from 3.6 s for BF3, to 5.3 s for BF4, which has the higher PIB concentration. $\lambda 2$ is slightly higher than λPB, but the values are in the same order of magnitude. This effect may be due to PIB, as an increase in PIB would also lead to an increase in $\lambda 2$.

Rheological properties of Co-PEPP were explored at different temperatures under protective gas. Figure 6 shows the master curve at 230 °C. This material shows a typical behaviour of viscoelastic polymer, with a Newtonian plateau at low frequencies, followed by a decrease in viscosity. Table 7 gives Newtonian viscosities and relaxation times determined at each temperature. Newtonian viscosities for sintering tests temperatures will be estimated by fitting data with an Arrhenius law.

Table 6 Zero-shear viscosities and relaxation times for the Boger fluids at 25 °C

Fluid	Eta*0 (Pa s)	λ (s)	λ (s)	λPB (s)
BF1	17	0.6	3.6×10^{-5} (1)	10^{-5}
BF2	30.8	0.9	10^{-4} (1)	
BF3	275	3.6	4×10^{-3}	2.6×10^{-3}
BF4	420	5.3	10^{-2}	

The relaxation times for PB used in each Boger fluid are recalled in column 5. Relaxation time was determined by Cole–Cole method, except for (1) which was estimated by a numerical simulation

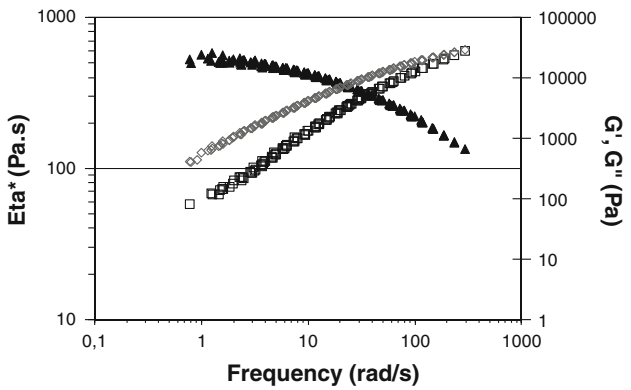

Fig. 6 Complex shear viscosity (*triangle*) and moduli vs frequency for Co-PEPP at 230 °C

Table 7 Zero-shear viscosities and relaxation times for Co-PEPP from 180 to 230 °C

Temperature (°C)	Newtonian viscosity (Pa s)	Relaxation time (s)
180	1980	0.79
190	1300	0.45
200	1150	0.39
210	930	0.32
220	680	0.25
230	600	0.20

The complex viscosities as a function of the frequency for PE, PE-G, PP and PP-G at 200 °C are shown in Figs. 7 and 8. The viscosity of PP shows a Newtonian plateau for low frequencies. The shear-thinning appears above 0.2 rad/s. Its Newtonian viscosity and relaxation time are shown in Table 8. PP-G does not seem to present any Newtonian plateau. Measures at low frequencies have a poor accuracy because of the lack of sensibility of the sensor. We also

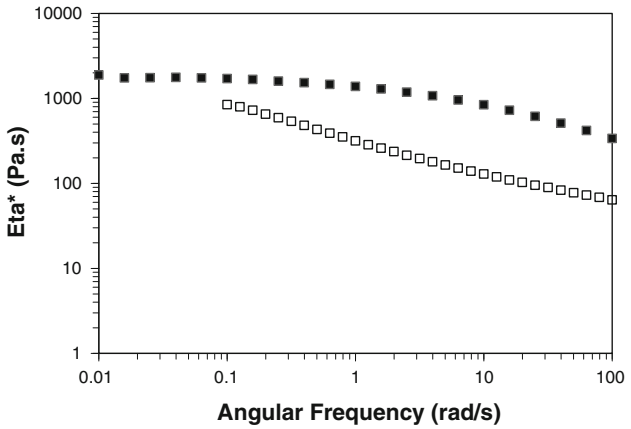

Fig. 7 Complex shear viscosity vs frequency for PP (*filled square*) and PP-G (*open square*) at 200 °C

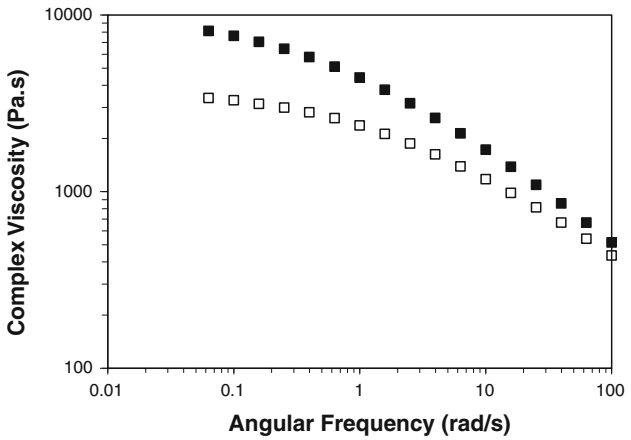

Fig. 8 Complex shear viscosity vs frequency for PE (*filled square*) and PE-G (*open square*) at 200 °C

Table 8 Zero-shear viscosities and relaxation times for PP, PP-G, PE and PE-G at 200 °C

Sample	Newtonian viscosity (Pa s)	Relaxation time (s)
PP	1850	0.15
PP-G	6232	3.9
PE	10,656	9.9
PE-G	4643	3.9

observe an increase of the viscosity. The zero-shear viscosity and relaxation time estimated by a fitting with Carreau model and indicated in Table 8 may be over estimated. PE and PE-G are highly viscous and elastic materials in comparison with Co-PEPP or PP. PE presents a zero-shear viscosity more than 10600 Pa s and a relaxation time about 10 s at 200 °C. PE-G is a little less viscous and elastic. We note that they show a beginning of a Newtonian plateau at low frequencies. We must carefully note that PE-G is sensitive to crosslinking, i.e., an increase of its viscosity under heat action. An inert gas allows us to reduce this effect, but will disrupt sintering tests.

Sintering kinetics

The observed evolution in shape during sintering was compared to Bellehumeur et al. model using the parameters obtained from the rheological tests, the surface tension measurements (γ) and the initial drop radius (r_0). The evolution of x/r as a function of time was obtained by integrating Eq. 1 using Runge–Kutta routine. It should be noted that it was impossible to measure the initial value of x/r. Therefore, the first x/r value obtained experimentally was taken as the initial value in the integration and in the worst case this value ranged between 0.25 and 0.35. For comparison purposes, the experimental data can also be fitted by the following simple expression when possible:

$$\frac{x}{r} = 1 - K\mathrm{e}^{-(t/\tau)} \tag{10}$$

From this fitting, the sintering time t_{99}, a characteristic time λ and the slope $\mathrm{d}(x/r)/\mathrm{d}t$ at the initial stage can be deduced. t_{99} can be reduced in order to take into account the zero-shear viscosity, the surface tension and the initial particle radius:

$$t_{\mathrm{r}} = \frac{t_{99}\gamma}{\eta_0 r_0} \tag{11}$$

Model fluids

Figures 9 and 10 represent the sintering curves for the 3 PDMS on a PTFE and copper substrate. All these fluids

have the same elastic parameters and similar surface tensions. We can also observe the effect of the viscosity on sintering kinetics [18]. PDMS1 coalesces faster than PDMS2 and PDMS3 on both PTFE and copper. Sintering times t_{99} and reduced sintering times t_r are shown in Table 9. On a PTFE substrate, only 6.2 s are necessary for PDMS to sinter totally against 14.7 and 42.3 s for PDMS2 and PDMS3. The same trend is observed on copper substrate. Reduced times t_r are similar between the three materials on a same substrate. This indicates that only viscosity, surface tension and initial particles radii play a role. Bellehumeur et al. model describes relatively well the experimental data.

Figures 11 and 12 represent the sintering kinetics for PB1 and PB2 on a PTFE and a copper substrate. As before, the less viscous material coalesces the faster, independently of the substrate. The comparison between experimental data and Bellehumeur et al. model for experiments on a PTFE substrate show that the model overestimates the sintering kinetic for PB2. To explain this phenomenon, we must focus on the interfacial tension. To quantify it, we can calculate the spreading parameter S as:

$$S = \gamma_S - (\gamma_L + \gamma_{SL}) \quad (12)$$

Table 10 gives the interfacial tension and spreading parameters on each substrate. As we can see, the spreading parameter for PB2 is negative. This signifies that the fluid will not wet the PTFE. Note that S is also negative for PB1 and the 3 PDMS. However, the model fits well the experimental data for these fluids. In fact, the sintering is governed by two contributions: (1) the wetting capacity and (2) the diffusion at the interface. For PB2, the wetting is unfavourable and the diffusion is slowdown because of its high viscosity. For PB1 and the PDMS, despite a negative spreading parameter, the diffusion is higher and this effect seems not to be affected by a low wetting capacity.

If we have a look in Fig. 12 (sintering on a copper substrate), we observe the same phenomenon as described

Table 9 Sintering times t_{99} and reduced sintering times t_r for model fluids on each substrate

Material	Sintering on PTFE		Sintering on copper	
	t_{99} (s)	t_r	t_{99} (s)	t_r
PDMS1	6.2	3.15	7.3	3.25
PDMS2	14.7	3.03	17.3	3.17
PDMS3	42.3	3.09	50.0	3.25
PB1	9.5	2.58	11.4	2.90
PB2	322.5	4.19	217.5	2.83
BF1	7.3	2.76	8.2	3.04
BF2	14.9	3.04	16.0	3.18
BF3	130.5	3.15	145.0	3.26
BF4	225.0	3.48	192.5	2.91

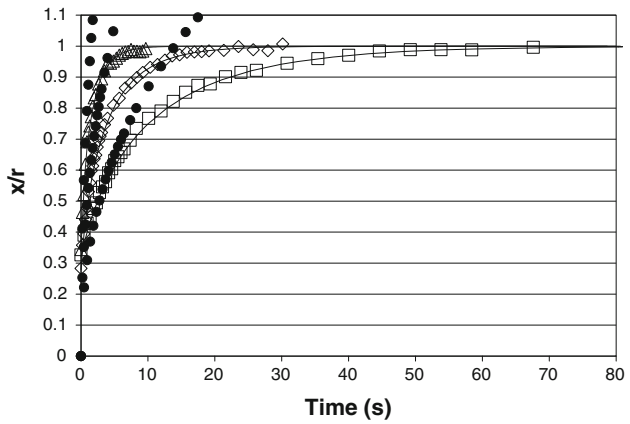

Fig. 9 Coalescence curves on PTFE for: PDMS1 (*triangle*), PDMS2 (*diamond*) and PDMS3 (*square*). The *solid lines* represent the Bellehumeur et al. model for each PDMS material and the *full circles* are the Frenkel's model

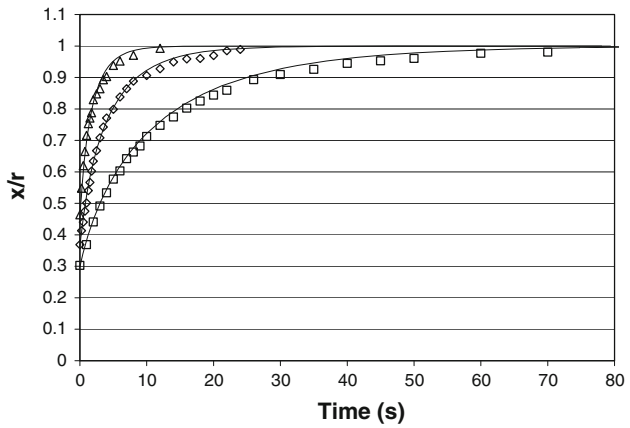

Fig. 10 Coalescence curves on copper for: PDMS1 (*triangle*), PDMS2 (*diamond*) and PDMS3 (*square*). The *solid lines* represent the Bellehumeur et al. model for each PDMS material

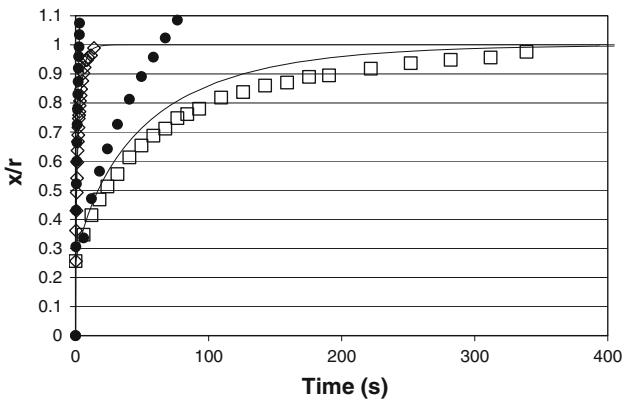

Fig. 11 Coalescence curves on PTFE for: PB1 (*diamond*) and PB2 (*square*). The *solid lines* represent the Bellehumeur et al. model for each PB material and the *full circles* are the Frenkel's model

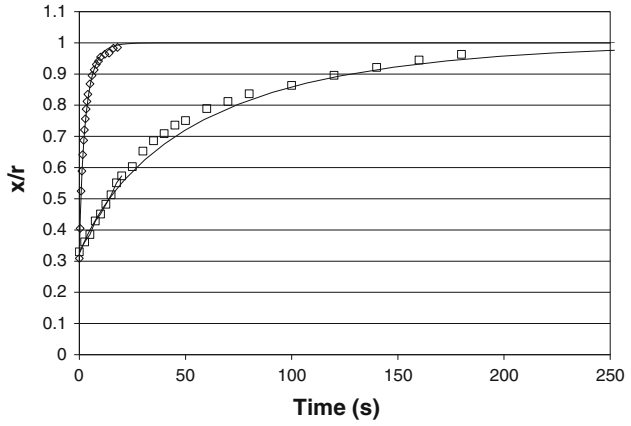

Fig. 12 Coalescence curves on copper for: PB1 (*diamond*) and PB2 (*square*). The *solid lines* represent the Bellehumeur et al. model for each PB material

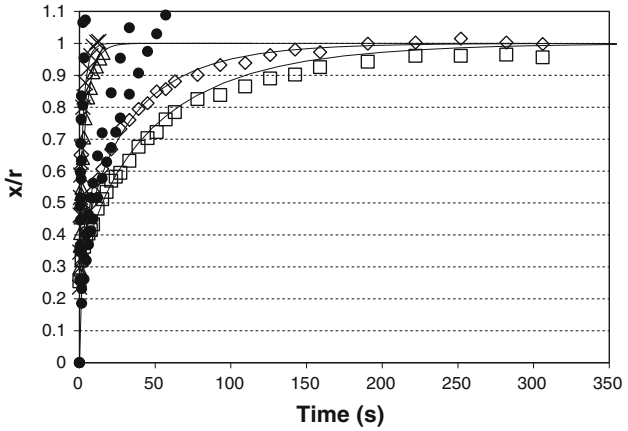

Fig. 13 Coalescence curves on PTFE for: BF1 (*cross*), BF2 (*triangle*), BF3 (*diamond*) and BF4 (*square*). The *solid lines* represent the Bellehumeur et al. model for each Boger fluid and the *full circles* are the Frenkel's model

above. The only difference is that the spreading parameter is positive for the materials. Bellehumeur et al. model describes relatively well the data for PB1. For PB2, the model underestimates the sintering kinetic. At the opposite of the case on a PTFE substrate, PB2 will wet the copper substrate. The sintering is also accelerated, which is not taken into account in the model. We have here shown that the interfacial tension plays a major role in the sintering process for the most viscous materials. Furthermore, the wetting capacity seems to be preponderant on the diffusion at the interface.

The sintering kinetics of BF's on a PTFE and a copper substrate are shown in Figs. 13 and 14. As we have seen, the interfacial tension plays a non-negligible role on the sintering process. To observe the effect of the elasticity, we will compare BF1 and BF2, then BF3 and BF4 since they have the same surface tension and equivalent viscosities. As before, the less viscous material coalesces the faster. The sintering time is 7.3 s for BF1 against 14.9 s for BF2 on a PTFE substrate. The sintering of BF3 is complete in 130.5 s while 225 s are necessary for BF4. The same orders of magnitude are observed on a copper substrate. Bellehumeur et al. model describes nicely the experimental points for BF1 and BF2 both on PTFE and copper. By contrast, we observe a deviation of the model for BF3 and BF4, as it was observed for PB2. We face again the effect of interfacial tension.

Now focus on the reduced sintering times t_r of BF1 and BF2. On a PTFE substrate, they raise from 2.76 to 3.04. On a copper one, $t_r = 3.04$ for BF1 and $t_r = 3.18$ for BF2. The only discriminating parameter which is not taken into account in the reduced time between these two fluids is their elasticity λ. We observe that an increase of the elasticity lead to an increase of the reduced time. We can also carry out the same analysis for BF3 and BF4 on a PTFE substrate. The reduced time increases from 3.15 to 3.48 for F3 and BF4, respectively. In the same time, their relaxation time increases from 3.6 to 5.3 s. As on PTFE, an increase of the relaxation time leads to a longer sintering time. We cannot conclude for the data on the copper substrate because the effect of the interfacial tension seems to be more important for BF4 than for BF3.

Table 10 Interfacial tensions and spreading parameters for model fluids on each substrate

Material	On a PTFE substrate		On a copper substrate	
	Interfacial tension (mN/m)	Spreading parameter (mN/m)	Interfacial tension (mN/m)	Spreading parameter (mN/m)
PDMS1	8×10^{-3}	−0.84	8.99	10.57
PDMS2	1.9×10^{-2}	−1.34	8.89	10.19
PDMS3	1.2×10^{-2}	−1.06	8.94	10.40
PB1	0.14	−3.91	8.44	8.19
PB2	0.24	−5.12	8.28	7.24
BF1	0.16	−4.12	8.41	8.03
BF2	0.15	−3.94	8.43	8.17
BF3	0.23	−4.95	8.30	7.38
BF4	0.24	−5.09	8.28	7.27

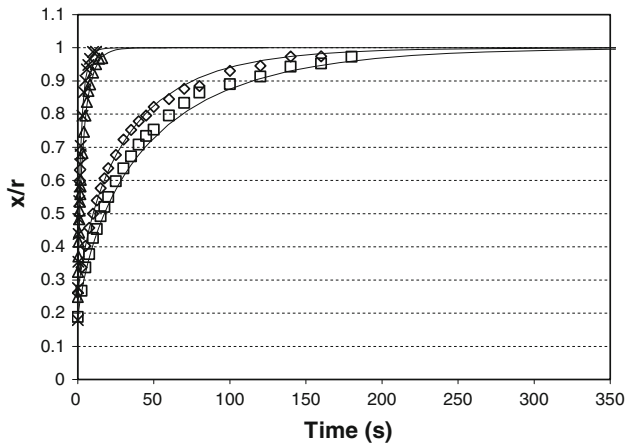

Fig. 14 Coalescence curves on copper for: BF1 (*cross*), BF2 (*triangle*), BF3 (*diamond*) and BF4 (*square*). The *solid lines* represent the Bellehumeur et al. model for each Boger fluid

To sum up, the sintering of polymer is mainly governed by the viscosity. The elasticity slows down the sintering rates. The interfacial tension plays a role for the more viscous materials at a same temperature and may accelerate or slow-down the kinetics depending of the wetting of the substrate.

Sintering of Co-PEPP

Figures 15 and 16 illustrate the sintering kinetics for Co-PEPP at 195 and 225 °C on a sapphire and a polyamide (PA) substrate. First, focus on the coalescence on the sapphire substrate. The Co-PEPP material coalesces faster at 225 °C than at 195 °C. This is mainly due to the decrease of its viscosity. The sintering at the two temperatures is nearly complete ($x/r \sim 1$). Bellehumeur et al. model describes relatively well the experimental data at 195 °C. However, we note a deviation of the model at 225 °C. It underestimates the sintering kinetic. We observe here the effect of the interfacial tension. The surface tension of the sapphire is higher than that of Co-PEPP. The spreading parameter S is also positive, i.e., the material will wet the substrate and the sintering will be accelerated. This phenomenon is more limited at 195 °C despite a highest viscosity. Indeed, we found with the model fluids that the effect of the interfacial tension can be seen for the material with a high viscosity. The fact is that the difference of viscosity between PB1 and PB2 is due to their difference in molecular weight. They are relatively low (Mn = 920 g/mol for PB1 and Mn = 2300 g/mol for PB2), so the possibility of movements for macromolecular chains are comparable. In the case of Co-PEPP, the molecular weight Mn is 48000 g/mol. The decrease in viscosity between 195 and 225 °C is due to a larger possibility of movements of the chains, not to a difference of Mn. The material will also spread easier at 225 °C than at 195 °C.

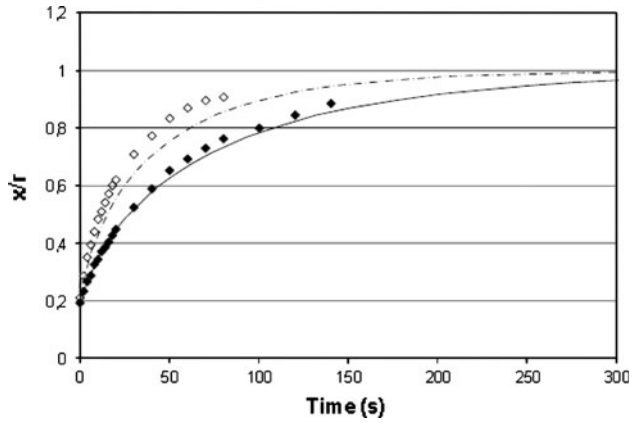

Fig. 15 Coalescence curves on sapphire for Co-PEPP at: 195 °C (*filled diamond*) and 225 °C (*open diamond*). The *solid lines* represent the Bellehumeur et al. model for each temperature

Now have a look on the sintering curves on a PA substrate as illustrated in Fig. 16. The surface tension of the polyamide is lower than that of Co-PEPP. Furthermore, the film of PA is in a solid state at 195 °C but is molten at 225 °C. We first observe that Bellehumeur et al. model failed totally to describe the experimental data. The shape of the experimental curve at 195 °C may be explained by the effect of the interfacial tension since the shift of the curve of the model is nearly constant. The polymer does not wet the PA film so the sintering is slowing down. For the test at 225 °C, another phenomenon seems to interact with the sintering kinetic. The coalescence is uncompleted (x/r tends toward 0.8). The particles of Co-PEPP disposed on the PA at 225 °C have the trend to settle into the film. They are frozen into the PA so that the sintering is not complete. If we compare the data at 195 and 225 °C, the kinetic is faster at 225 °C at the beginning of the experiment. After 30 s, its kinetic strongly slows down. At the end of the experiment, the global kinetic at 195 °C is faster than that at 225 °C despite a lowest viscosity. We have

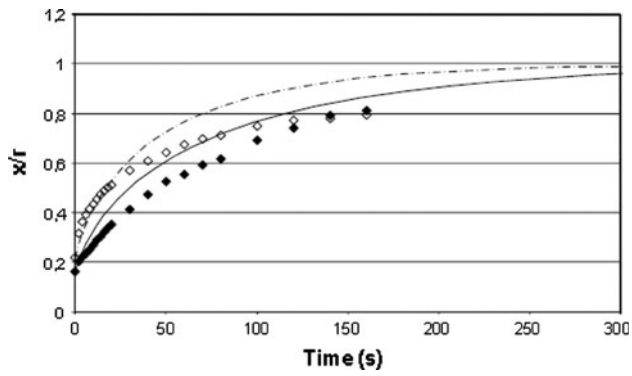

Fig. 16 Coalescence curves on polyamide for Co-PEPP at: 195 °C (*filled diamond*) and 225 °C (*open diamond*). The *solid lines* represent the Bellehumeur et al. model for each temperature

here shown that the physical state of the substrate may be a primary parameter on the sintering.

Sintering of PP and PP-G

The study of the sintering kinetics of PP and PP-G was carried out only at 200 °C on the two same substrates that Co-PEPP. Figure 17 shows these kinetics. The first remark we can formulated is that PP-G coalesces faster than PP, especially at the beginning of the experiment. It is quite surprising since the zero-shear viscosity of PP is lower than that of PP-G. As we have mentioned before, the zero-shear viscosity of PP-G may be overestimated because experimental errors. Furthermore, Bellehumeur et al. model does not describe at all the experimental data of PP-G. To solve this problem we can calculate the initial sintering strain rate between t_1 and t_2 by:

$$\dot{\varepsilon}_i = \frac{(x_2 - x_1)}{x_2}\frac{1}{t_2 - t_1} \tag{13}$$

It appears that $\dot{\varepsilon}_i$ ranges 0.07 from 0.13 s^{-1} for PP and PP-G. The idea is to use the viscosity at 0.1 rad/s instead the zero-shear viscosity. For the PP material $\omega = 0.1$ is equal to its zero-shear viscosity. For PP-G the viscosity at 0.1 rad/s is equal to 847 Pa s. We can now replace $\omega = 0$ by $\omega = 0.1$ in Bellehumeur et al. model.

Figure 18 represents the model with $\omega = 0.1$. As we discussed before, PP-G coalesces faster than PP. The viscosity at 0.1 rad/s is 1850 Pa s for PP against 847 Pa s for PP-G. Beyond 100 s the sintering kinetics are quite similar for the two materials on the sapphire substrate. We note a slowdown of the sintering for PP-G which may be due to a beginning of auto-crosslinking or degradation of the material. We found again the trend observed with the Co-PEPP material on a PA substrate. The sintering is slowing down on a non-wetting substrate. Despite the particles are on a solid surface at 200 °C, their coalescence is uncompleted. This can be explained by their relatively high viscosity. Furthermore, the sintering kinetics on PA and on sapphire are very close at the very start of the experiments. The effect of the interfacial tension seems to be preponderant only after a certain time, i.e., for low strain rates.

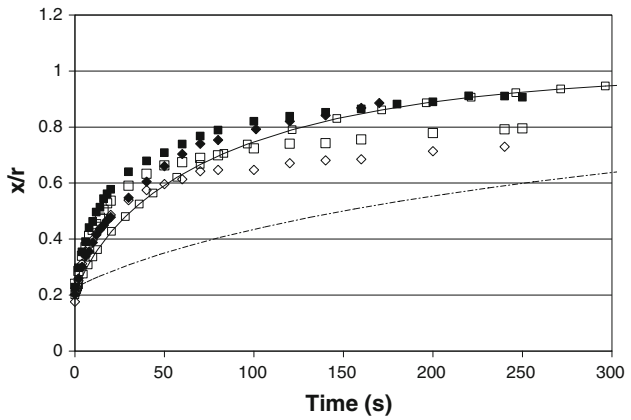

Fig. 17 Coalescence curves of PP (*filled diamond*, *open diamond*) and PP-G (*filled square*, *open square*) on sapphire (*filled diamond*, *filled square*) and on polyamide (*open diamond*, *open square*) substrates at 200 °C. Bellehumeur et al. model for PP is in full line that for PP-G is represented by a *dashed line*

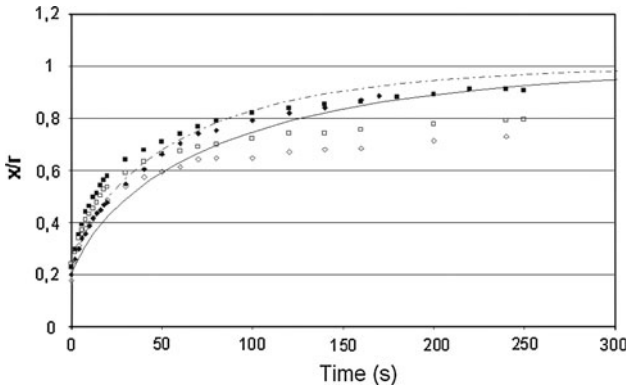

Fig. 18 Coalescence curves of PP (*filled diamond*, *open diamond*) and PP-G (*filled square*, *open square*) on sapphire (*filled diamond*, *filled square*) and on polyamide (*open diamond*, *open square*) substrates at 200 °C. Bellehumeur et al. model for PP is in full line that for PP-G is represented by a *dashed line*. The zero-shear viscosity has been replaced by the viscosity at 0.1 rad/s into the models

Bellehumeur et al. model shown in Fig. 18 describes the order of magnitude of the sintering kinetics of PP-G on a sapphire substrate better than that shown in Fig. 17. However, the models underestimate the kinetics especially at the beginning of the experiment. For long times, the model over estimates the sintering. Bellehumeur et al. model failed totally to describe the experimental data on a PA substrate since the interfacial tension effect is not taken into account in the model.

Sintering of PE and PE-G

The sintering of PE and PE-G has been studied at 200 °C on a sapphire and a PA substrate. Figure 19 represents the results obtained. As for PP-G, Bellehumeur et al. model fails to describe the sintering kinetics. The initial sintering strain rate is about 0.1 s^{-1}. We an here again use the viscosity at 0.1 rad/s instead the zero-shear viscosity into the model. Figure 20 shows the model corrected with this viscosity. It is a bit closer of the experimental data but it is still along to predict the kinetics.

Compare now the sintering of PE and PE-G on a sapphire substrate. PE coalesces faster than PE-G. This is also surprising since PE has a higher viscosity than PE-G. Furthermore, the coalescence of PE-G is not complete since x/r tends to 0.9. We attribute that to the auto-crosslinking of this material. Despite the protective gas we cannot suppress totally

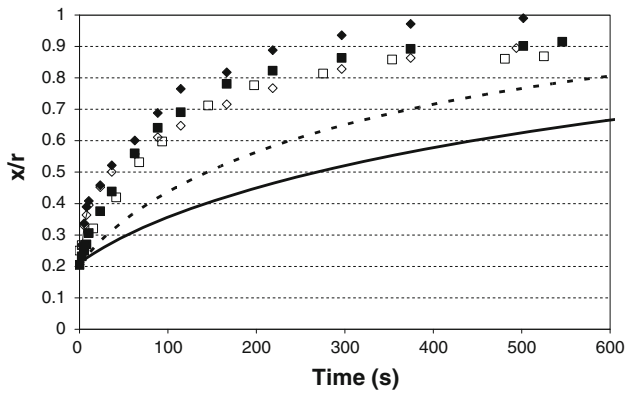

Fig. 19 Coalescence curves of PE (*filled diamond*, *open diamond*) and PE-G (*filled square*, *open square*) on sapphire (*filled diamond*, *filled square*) and on polyamide (*open diamond*, *open square*) substrates at 200 °C. Bellehumeur et al. model for PE is in full line that for PE-G is represented by a *dashed line*

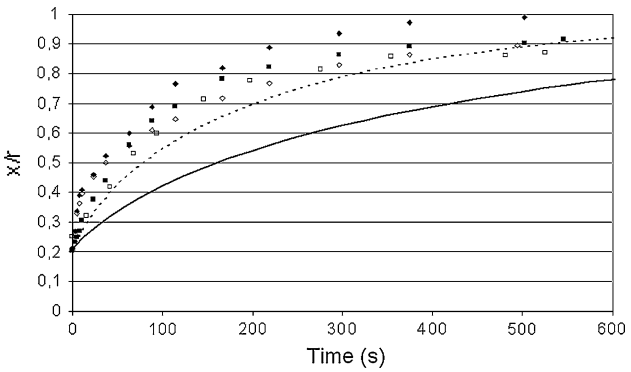

Fig. 20 Coalescence curves of PE (*filled diamond*, *open diamond*) and PE-G (*filled square*, *open square*) on sapphire (*filled diamond*, *filled square*) and on polyamide (*open diamond*, *open square*) substrates at 200 °C. Bellehumeur et al. model for PE is in full line that for PE-G is represented by a *dashed line*. The zero-shear viscosity has been replaced by the viscosity at 0.1 rad/s into the models

this phenomenon. The viscosity increases and the sintering is slowing down. If we have a look on kinetics on a PA substrate we observe that they are similar of that on a sapphire one at the very start of the experiment. As it was mentioned before, the effect of the interfacial tension seems appear for lowest strain rates. PE coalesces faster than PE-G, maybe because of auto-crosslinking as on sapphire. For long times (here >100 s), the kinetics for the two materials are quite comparable. The coalescence is uncompleted since their final x/r is mostly equal to 0.85–0.9, which is lower to that on a sapphire substrate. One more time, the fact of being on a non-wetting surface for these materials disadvantages the coalescence.

Concluding remarks

We have in this study shown that several parameters influence the coalescence of polymers. The most important is the viscosity which slows down the sintering rates when it increases. The elasticity of the material is also unfavourable for the sintering. We point out another parameter that plays a role on the sintering kinetics which is the interfacial tension. On a wetting substrate the particles will have tendency to coalesce faster. On the contrary, the sintering rate will decreases on a non-wetting one. This phenomenon is closely linked to the viscosity and the molecular weight of the material. We also observed other phenomena, like thermal degradation or crosslinking, which in most of the case will slow down the sintering kinetics and lead to incomplete coalescence. The experimental data were compared with Bellehumeur et al. model. The model describes relatively well the sintering for Newtonian materials at low frequencies. The zero-shear viscosity may not appropriated for non-Newtonian materials. We found that the viscosity at 0.1 rad/s may be better to describe the sintering process. Finally, the model failed to take into account the effect of the interfacial tension. A modification of the model may improve its accuracy, but will decrease its relative simplicity. In conclusion, this fundamental study on sintering is widely applicable to many net-shape manufacturing processing.

References

1. Perot E, Maazouz A (2007) J Polym Eng 27(4):267
2. Kuczynski GC (1972) Adv Colloid Interface Sci 3:275
3. Rahaman NM (2003) Ceramic processing and sintering. Marcel Dekker, New York
4. Mazur S (1995) Polymer powder technology. Wiley, New York
5. Frenkel J (1945) J Phys 9:385
6. Eshelby (1949) J Metals 1:806
7. Hopper J (1984) Am Ceram Soc 67:C262
8. Pokluda O, Bellehumeur CT, Vlachopoulos J (1997) AlChE J 43:3253
9. Bellehumeur CT, Kontopoulou M, Vlachopoulos J (1998) Rheol Acta 37:270
10. Joseph DD (1990) Fluid dynamics of viscoelastic liquids. Springer, New York
11. Scribben E, Aaron PR, Baird GD (2005) J Rheol 49:1159
12. Boger DV (1977) J Non-Newton Fluid Mech 3:87
13. Owens DK, Wendt RCJ (1969) Appl Polym Sci 13:1741
14. Tinson A (2004) M.A.Sc Thesis, McMaster University
15. Kwak DY, Cheung LK, Park CB, Neumann AW (1998) Polym Eng Sci 38(5):757
16. Wu S (1982) Polymer interface and adhesion. Marcel Dekker, New York
17. Hata T, Kasemura T (1980) In: Lee LH (ed) Adhesion and adsorption of polymers, vol 12a. Plenum Press, New York, p 15
18. Muller J-D, Bousmina M, Maazouz A (2008) Macromolecules 41(6):2096